Black hole dynamics in Einstein-Maxwell-dilaton theory

Eric W. Hirschmann,[1] Luis Lehner,[2] Steven L. Liebling,[3] and Carlos Palenzuela[4]
[1]*Brigham Young University, Provo, Utah 84602, USA*
[2]*Perimeter Institute for Theoretical Physics, Waterloo, Ontario N2L2Y5, Canada*
[3]*Long Island University, Brookville, New York 11548, USA*
[4]*Departament de Fısica & IAC3, Universitat de les Illes Baleares and Institut d'Estudis Espacials de Catalunya, Palma de Mallorca, Baleares E-07122, Spain*

(Received 29 August 2017; published 26 March 2018)

We consider the properties and dynamics of black holes within a family of alternative theories of gravity, namely Einstein-Maxwell-dilaton theory. We analyze the dynamical evolution of individual black holes as well as the merger of binary black hole systems. We do this for a wide range of parameter values for the family of Einstein-Maxwell-dilaton theories, investigating, in the process, the stability of these black holes. We examine radiative degrees of freedom, explore the impact of the scalar field on the dynamics of merger, and compare with other scalar-tensor theories. We argue that the dilaton can largely be discounted in understanding merging binary systems and that the end states essentially interpolate between charged and uncharged, rotating black holes. For the relatively small charge values considered here, we conclude that these black hole systems will be difficult to distinguish from their analogs within General Relativity.

DOI: 10.1103/PhysRevD.97.064032

I. INTRODUCTION

One particularly exciting prospect arising from the recent advent of gravitational wave astronomy is the possibility of testing General Relativity (GR) in the previously inaccessible strongly gravitating/highly dynamical regime. Indeed, first steps in this direction have already been enabled by the first three available detections: GW150914 [1], GW151226 [2], and GW170104 [3]. Analysis of these signals reveals that they are consistent with those produced by black hole mergers in GR [4,5], with independent and complementary tests coming from the inspiral and post-merger periods.

Ongoing efforts with additional detections and studies of predicted signals will allow for further scrutiny [6–8]. Accurate predictions of possible signals are not only important to aid in future detections but are also helpful in realizing important tests of the theory. Such tests could potentially indicate that nature deviates from GR. However, simply identifying possible deviations is unlikely to provide sufficient guidance as to the alternative that nature may have chosen. In contrast to the GR case, our understanding of potential signals within alternative theories of gravity is still rather limited.

To date, this approach of looking for such deviations has been primarily restricted to the consideration of phenomenological models (e.g. Refs. [9,10]). Another avenue for obtaining detailed predictions is to use fully nonlinear treatments within specific alternative gravitational theories. Such an approach, however, requires theories which possess well-posed evolutionary problems in addition to producing spacetime deviations in, for example, binary black hole mergers. Such a requirement is fairly stringent and limits the number of possible options. We do note that there is a body of previous work which has studied the possibility of deviations within the context of binary neutron star systems (see e.g. Refs. [11–14]). However, currently available observations indicate that the majority of events that we might expect in the near future should correspond to binary black hole systems [15]. Recent approaches to the nonlinear regime for such binary mergers in GR alternatives are beginning to address concerns with, for example, ill-posedness [16–18].

In the present work, we study black hole systems (single and binaries) in the Einstein-Maxwell-dilaton (EMD) theory [19]. This theory, originating from a low energy limit of string theory, allows for black holes that have mass, rotation, charge and scalar "hair" together with scalar, vector, and tensor radiative channels. Furthermore, its mathematical structure allows for defining a well-posed initial value problem. It therefore offers an interesting theoretical and computational playground within which to explore possible deviations from the Standard Model (i.e. GR) prediction.

While we provide below some specifics regarding the black holes we consider in this work, it is worth mentioning that our understanding of black hole systems in EMD is admittedly rather limited. For example, analytic solutions are known primarily for nonrotating systems. A spherically symmetric family of solutions parametrized by the scalar (dilaton) coupling exists, and these solutions are known

analytically across a range of coupling values. However, analytic investigations of their perturbations, stability, and rotating generalizations are at best limited to a handful of specific values of the coupling.

While our aim in the current work is not necessarily to address all of these questions, we do study single and binary black hole systems within EMD and draw some general conclusions to help understand the dynamics of coalescing binaries.

The subsequent presentation is divided up as follows. Section II presents the equations of motion describing the systems' dynamics. Section III includes a brief description of known, nonspinning black holes, possible instabilities, and a discussion of possible radiative effects. Section IV presents results for both single and binary black hole systems for the case of small charge. We conclude in Sec. V. We defer to an Appendix a description of EMD black hole solutions in isotropic coordinates and to a second Appendix a calculation of the radiative properties in the Jordan frame.

II. EQUATIONS

The alternative theory of gravity that we consider has origins in low energy string theory. A particular sector of this theory includes a U(1) gauge field and a scalar field that couples exponentially to the gauge field. For definiteness, we consider the action for low energy, heterotic string theory

$$S = \int d^4x\sqrt{-\tilde{g}}e^{-2\phi}\left[R + \Lambda + 4(\nabla\phi)^2 - F^2 - \frac{H^2}{12}\right], \quad (1)$$

where the matter content includes a scalar field serving as the dilaton, ϕ; a U(1) gauge field, F_{ab}; and a three-form field, H_{abc}, which is related to the axion and which, together with the cosmological constant Λ, we set to zero in the following. This action is written with respect to the string metric, $\tilde{g}_{ab}$, which is the metric to which strings couple. (It is also referred to as the Jordan metric or frame.) In many treatments, including this work, a conformal transformation is performed to the Einstein metric, or frame, via $g_{ab} = e^{-2\phi}\tilde{g}_{ab}$. On performing this transformation at the level of the action, we arrive at the expression

$$S = \int d^4x\sqrt{-g}\left[R - 2(\nabla\phi)^2 - 2V - e^{-2\alpha_0\phi}F^2\right], \quad (2)$$

where, as before, the scalar field, ϕ, is the dilaton and F_{ab} is the Maxwell tensor. Note that we have chosen to generalize the theory a bit by including $V(\phi)$, a potential for the dilaton, together with including the real constant α_0 to parametrize among theories. In particular, $\alpha_0 = 0$ is just Einstein-Maxwell minimally coupled to a real scalar field, $\alpha_0 = 1$ is the sector of low energy string theory referred to above, and $\alpha_0 = \sqrt{3}$ corresponds to Kaluza-Klein theory [20,21]. This action defines a class of theories often referred to as Einstein-Maxwell-dilaton. Our interest focuses on dynamical processes within this theory and how they might compare with standard General Relativity.

The equations of motion that follow from this action are the Einstein-Maxwell equations coupled nonlinearly to a propagating scalar field (the dilaton), namely

$$R_{ab} = 2\left(T_{ab} - \frac{1}{2}g_{ab}T\right) \quad (3)$$

$$\nabla^a\nabla_a\phi = \frac{1}{2}\frac{\partial V}{\partial\phi} - \frac{\alpha_0}{2}e^{-2\alpha_0\phi}F^2 \quad (4)$$

$$\nabla^a F_{ab} = -I_b. \quad (5)$$

Notice that the exponential coupling of the dilaton in its equation of motion is again present in both the four-current, I_b, and the stress-energy tensor

$$I_b = -2\alpha_0\nabla^a\phi F_{ab} \quad (6)$$

$$T_{ab} = T^{\phi}_{ab} + e^{-2\alpha_0\phi}T^{\rm EM}_{ab} \quad (7)$$

$$T^{\phi}_{ab} = \nabla_a\phi\nabla_b\phi - \frac{1}{2}g_{ab}[\nabla_c\phi\nabla^c\phi + V(\phi)] \quad (8)$$

$$T^{\rm EM}_{ab} = F_{ac}F_b{}^c - \frac{1}{4}g_{ab}F^2. \quad (9)$$

These equations are supplemented by the identity $\nabla_{[a}F_{bc]} = 0$. Because of the presence of this and related constraint equations in the above evolution system, we, in fact, use an extended Maxwell system which aids in damping dynamically these constraints. To the above Maxwell equations, we add extra scalar fields, Ψ and Φ, in such a way that the Maxwell constraints are allowed to propagate at the speed of light. These equations become

$$\nabla^a(F_{ab} + g_{ab}\Psi) = \kappa_1 n_b\Psi - I_b \quad (10)$$

$$\nabla^a((*F)_{ab} + g_{ab}\Phi) = \kappa_2 n_b\Phi, \quad (11)$$

where the κs are real constants used to adjust the constraint damping and $(*F)_{ab} = \frac{1}{2}\epsilon_{abcd}F^{cd}$ is the dual of F_{ab}.

We use the usual Cauchy, or $3+1$, decomposition in which the spacetime is foliated into spacelike hypersurfaces, Σ_t, labeled by a coordinate time, t. The timelike normal is n^a with orientation such that $n_a = -\alpha\delta^t_a$, and the metric on the hypersurfaces is γ_{ij}. The lapse and vector shift of the coordinates are given by α and β^i. The line element of the spacetime is then

$$ds^2 = -\alpha^2 dt^2 + \gamma_{ij}(dx^i + \beta^i dt)(dx^j + \beta^j dt). \quad (12)$$

Note that we define a derivative operator, D_i, built from the 3-metric γ_{ij}, which should be compared with the full derivative operator, ∇_a, built from g_{ab}. Likewise, we define a 3-Levi-Cività antisymmetric tensor density as $\epsilon_{bcd} = n^a \epsilon_{abcd}$.

With respect to these $3+1$ variables, we can write the above matter equations as

$$(\partial_t - \mathcal{L}_\beta)\phi = -\alpha\Pi \tag{13}$$

$$(\partial_t - \mathcal{L}_\beta)\Pi = -D^i(\alpha D_i\phi) + \alpha K\Pi + \frac{\alpha}{2}\frac{\partial V}{\partial\phi} - \alpha_0\alpha e^{-2\alpha_0\phi}[B_iB^i - E_iE^i] \tag{14}$$

$$(\partial_t - \mathcal{L}_\beta)E^i = \epsilon^{ijk}D_j(\alpha B_k) + \alpha[KE^i - D^i\Psi] - 2\alpha_0\alpha[\epsilon^{ijk}D_j\phi B_k + \Pi E^i] \tag{15}$$

$$(\partial_t - \mathcal{L}_\beta)\Psi = \alpha[2\alpha_0 D_j\phi E^j - D_jE^j - \kappa_1\Psi] \tag{16}$$

$$(\partial_t - \mathcal{L}_\beta)B^i = -\epsilon^{ijk}D_j(\alpha E_k) + \alpha[KB^i + D^i\Phi] \tag{17}$$

$$(\partial_t - \mathcal{L}_\beta)\Phi = \alpha[D_jB^j - \kappa_2\Phi], \tag{18}$$

where we define the electric, $E_i \equiv \gamma_i{}^j F_{jc} n^c$, and magnetic, $B_i \equiv \frac{1}{2}\epsilon_{ijk}F^{jk}$, fields relative to their projections into the spacelike hypersurface, Σ_t. Note, too, that we have defined $\Pi \equiv -n^a\nabla_a\phi$ and invoked the Lie derivative along the shift, $\mathcal{L}_\beta$.

For the evolution of the gravitational field in the Einstein frame, we use the BSSN formalism for which we give here only the projections of the matter stress tensor, namely

$$\rho = n^a n^b T_{ab} = D_i\phi D^i\phi + \Pi^2 + V + e^{-2\alpha_0\phi}(B_iB^i + E_iE^i) \tag{19}$$

$$j_i = -n^a\gamma_i{}^b T_{ab} = -2\Pi D_i\phi - 2e^{-2\alpha_0\phi}\epsilon_{ijk}E^jB^k \tag{20}$$

$$S_{ij} = \gamma_i{}^a\gamma_j{}^b T_{ab} = 2D_i\phi D_j\phi + 2e^{-2\alpha_0\phi}(B_iB_j - E_iE_j) - \gamma_{ij}[D^k\phi D_k\phi - \Pi^2 + V + e^{-2\alpha_0\phi}(B_kB^k - E_kE^k)]. \tag{21}$$

We implement the resulting equations using techniques described previously [22–27] and demonstrate convergence for a particular case as seen in Fig. 1. We note that we adopt the "1 + log" and Gamma drivers for the lapse function and the shift vector. Finally, using standard BSSN notation, we set the quantities K_0 and η to 0 and $2/M(1/M)$, respectively, for the single (binary) black holes studied here [28].

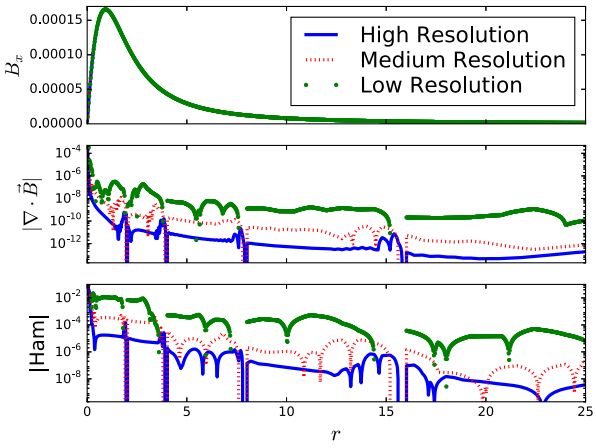

FIG. 1. Convergence for a magnetic black hole. Shown are various fields at late time ($t = 80M$) for three different resolutions. Each run uses fixed mesh refinement but differs by a factor of 2x in resolution for the same grid structure. The top panel shows that all three resolutions approach the same, static solution. The bottom two panels are measures of errors demonstrating that higher resolution runs have lower errors. In particular, the middle frame shows the divergence of the magnetic field which should be zero except at the center (because of the monopole charge). The bottom frame shows the residual of the Hamiltonian constraint.

III. PRELIMINARIES

Before discussing the dynamics as revealed by numerical evolutions, we first discuss some properties of the model.

A. Known black hole solutions

There exist a number of black hole solutions in EMD. One such solution is a static, magnetically charged black hole solution found in Refs. [19,29]. In Schwarzschild-like coordinates, this solution takes the form

$$ds^2 = -\left(1 - \frac{r_+}{r}\right)\left(1 - \frac{r_-}{r}\right)^{1-\alpha_1}dt^2 + \left(1 - \frac{r_+}{r}\right)^{-1}\left(1 - \frac{r_-}{r}\right)^{\alpha_1 - 1}dr^2 + r^2\left(1 - \frac{r_-}{r}\right)^{\alpha_1}d\Omega^2 \tag{22}$$

$$F_{\theta\phi} = Q_m \sin\theta \tag{23}$$

$$e^{-2\alpha_0\phi} = e^{-2\alpha_0\phi_0}\left(1 - \frac{r_-}{r}\right)^{\alpha_1}, \tag{24}$$

where $\alpha_1 = 2\alpha_0^2/(1+\alpha_0^2)$ and ϕ_0 is the asymptotic value of the dilaton at spatial infinity. This solution has magnetic charge Q_m. The constants $r_\pm$ are given in terms of Q_m, ϕ_0, and the ADM mass, M, of the spacetime:

$$2M = r_+ + (1 - \alpha_1)r_- \tag{25}$$

$$2Q_m^2 = e^{2\alpha_0\phi_0} r_+ r_- (2-\alpha_1). \tag{26}$$

Properties of this black hole solution are given, for instance, in Refs. [19,30]. For our purposes, it suffices to note that r_+ corresponds to an event horizon and r_- is the location of a curvature singularity. Note, too, that the dilaton, for $r > r_-$, is larger than its asymptotic value and monotonically decreases toward ϕ_0.

There is a discrete electromagnetic duality in this theory that exchanges magnetic and electric solutions. The explicit duality leaves the metric unchanged but sends $F_{ab} \to e^{-2\alpha_0\phi}(*F)_{ab}$ and $\phi \to -\phi$. Because of the presence of the dilaton, the electrically charged solution is, in fact, a different solution. While the metric takes the same form as above, the Maxwell field and dilaton become

$$F_{tr} = \frac{Q_e}{r^2} \tag{27}$$

$$e^{2\alpha_0\phi} = e^{2\alpha_0\phi_0}\left(1 - \frac{r_-}{r}\right)^{\alpha_1}, \tag{28}$$

for which the constants $r_\pm$ satisfy

$$2M = r_+ + (1-\alpha_1) r_- \tag{29}$$

$$2Q_e^2 = e^{-2\alpha_0\phi_0} r_+ r_- (2-\alpha_1). \tag{30}$$

In this case, the solution has electric charge, Q_e; ADM mass, M; asymptotic dilaton value, ϕ_0; an event horizon at $r = r_+$; a curvature singularity at r_-; and, for $r > r_-$, a dilaton monotonically increasing toward ϕ_0.

We know of linearized perturbations of these black holes only for the case $\alpha_0 = 1$ [31]. There quasinormal spectra have been computed, and it was shown that the presence of the dilaton induces a difference in the spectra of axial and polar perturbations. This difference breaks isospectrality, a property known to apply to both Schwarzschild and Reissner-Nordström (RN) black holes.

Note that in the limit $\alpha_0 \to 0$ the solution corresponds to that of a charged RN black hole. As $\alpha_0 \to \infty$, the solution is simply an uncharged Schwarzschild black hole for which the Maxwell field is zero and the dilaton is a constant. By extension, we expect (and show below) that for the rotating solutions α_0 interpolates between the charged Kerr-Newman black hole and the uncharged Kerr solution, the latter unadorned by scalar or vector fields. One way of understanding the $\alpha_0 \to \infty$ limit is that the gravitational sector decouples from the matter sector (see, for example, Ref. [32]). In this limit, regardless of the behavior of the dilaton and Maxwell field, the gravitational solutions are just those of GR, such as Schwarzschild and Kerr black holes.

Moving away from spherical symmetry, there are rotating black hole solutions in EMD, but to our knowledge, an analytic solution is only known for the case $\alpha_0 = \sqrt{3}$, which corresponds to Kaluza-Klein. Rotating, electrically charged solutions were constructed in Ref. [20] with dyonic generalizations described in Refs. [33,34]. Rotating solutions in EMD for other coupling values have been constructed numerically [35–37]. Further, the behavior of perturbations and questions related to stability would appear to be largely unexplored. An important exception to this is Ref. [31], which considers the quasinormal modes of the spherically symmetric solutions for $\alpha_0 = 1$. Recently, time-dependent, spherically symmetric solutions sourced by a charged null dust flow have been presented in EMD [38]. Interestingly, it is only for the coupling $\alpha_0 = 1$ that the solution describes a time-dependent dilaton (in addition to time-dependent metric and gauge fields). Although it includes an axion which we do not consider in this work, we note that quasinormal modes for the charged, rotating Kerr-Sen black hole have been considered in Refs. [39,40].

In what follows, we study both single and binary black hole scenarios and derive general statements about the dynamical behavior induced by EMD. As a prelude, we first present a simple-minded picture which can capture a possible transition in the behavior of the scalar field.

B. Scalar field instabilities

Here, we argue two types of instabilities could trigger nontrivial behavior of the scalar field. The analysis follows closely the arguments presented in Ref. [41].

Consider the linearized equation of motion for the dilaton, Eq. (4), which becomes

$$\Box\phi = -\frac{\alpha_0}{2}(1 - 2\alpha_0\phi) F^2 \tag{31}$$

with $\Box$ defined with respect to a background metric. We can rewrite the above equation as

$$(\Box - \mu^2)\phi = -\frac{\alpha_0}{2} F^2 \tag{32}$$

by introducing $\mu^2 \equiv \alpha_0^2 F^2$. Following the discussion in Appendix A, notice that μ^2 can have either sign, depending on whether the magnetic or electric field dominates. Assuming the charge Q (either magnetic or electric case) is small, the metric is that of Schwarzschild to $\mathcal{O}(Q^2)$. Expanding the dilaton in spherical harmonics as $\phi = \Sigma_{lm} e^{-i\omega t} Y_{lm}(\theta,\varphi)\Phi_{lm}(r)/r$ yields

$$f^2\Phi''_{lm} + f' f \Phi'_{lm} + [\omega^2 - f\bar{V}(r)]\Phi_{lm} = -f\frac{\alpha_0}{2} F^2 r e^{i\omega t} \tag{33}$$

with $\bar{V}(r) = l(l+1)/r^2 + 2M/r^3 + \mu^2$ and $f(r) = 1 - 2M/r$. This equation is similar to that obtained in Ref. [41] except for the presence of a source term on the right-hand side which is independent of Φ_{lm}. Integrating the equation over a period does away with the source, and in this cycle-averaged sense, we will ignore it in the following. A sufficient condition for an instability is that $\int_{r_{\rm BH}}^{\infty} \bar{V}(r) dr < 0$, which translates into

$$\int_{r_{\rm BH}}^{\infty}\left[\frac{l(l+1)}{r^2}+\frac{2M}{r^3}\right]dr<-\alpha_0^2\int_{r_{\rm BH}}^{\infty}F^2dr, \quad (34)$$

and thus the instability condition becomes

$$\frac{2l(l+1)+1}{4M}<-\alpha_0^2\int_{r_{\rm BH}}^{\infty}F^2dr. \quad (35)$$

Condition (35) implies that the electrically dominated case is subject to this instability while the magnetically dominated case is not. Indeed, such an instability resembles the standard negative mass instability, and that will be our primary focus here. However, we note that the magnetically dominated case may be subject to a superradiant type instability associated with rotating black holes as the effective mass μ could introduce a potential barrier that would provide feedback for such a process.

For now, consider Eq. (35) and evaluate it in a simple case such as the solution provided in Appendix A concentrating on the electrically dominated case and for small charge. Evaluation of Eq. (35) gives

$$\frac{2l(l+1)+1}{4M}<\alpha_0^2\frac{Q_e^2}{12M^3}, \quad (36)$$

for which the smallest bound on α_0 is achieved with $l=0$. Clearly, the coupling and charge must satisfy

$$3<\alpha_0^2\left(\frac{Q_e}{M}\right)^2. \quad (37)$$

On rearranging, this condition, $\alpha_0>\sqrt{3}(M/Q_e)$, indicates an instability at a large value of α_0 for small charges. This analysis suggests that one needs "large parameters to get large effects." For concreteness, a charge of $Q_e/M=10^{-3}$ predicts an instability for $\alpha_0\gtrsim 1.7\times 10^3$.

C. Extra degrees of freedom and black hole binaries

Although EMD is interesting in its own right, the remarkable direct detections of the mergers of black hole binaries by LIGO provides arguably the first opportunity to truly test gravity in strong field/highly dynamical settings. As such, we can regard EMD as an alternative to GR, one that includes additional degrees of freedom in the form of a scalar and vector field. In that respect, EMD has a scalar degree of freedom in common with scalar-tensor theories where several new phenomena have been well established.

In such theories, one can characterize the scalar field by its *scalar monopole charge*. This scalar charge (one generally drops the "monopole") can be evaluated by computing the divergence of the field over some large Gaussian surface. In particular, at large radius, one considers the behavior of the scalar as $\phi(r)\approx\phi_0+\phi_1/r$ so that ϕ_1 is the scalar charge and ϕ_0 is the asymptotic value of the scalar field.

In some scalar-tensor gravity theories, it has been found that the scalar field can grow significantly around compact neutron stars [42,43]. This process, known as *spontaneous scalarization*, induces a scalar charge around each neutron star that determines the extent to which the theory's predictions differ from those of GR [42,44]. In particular, such effects, originating in the scalar field, allow for an enhancement of the gravitational force and for additional channels of radiation (such as dipole scalar radiation). As a result, one generally expects such binaries to merge earlier than their GR counterparts (e.g. Refs. [11,14,43,45]). Black holes in such theories are identical to those of GR, and the gravitational waves observed in their merger provide no new features and therefore offer no distinguishing test of the theory (unless the asymptotic value of the scalar field is time dependent [46]).

In contrast, the EMD gravity theory that we study here allows for a scalar charge even without the presence of matter as long as the gauge field (and thus the gauge charge of the black hole) is nonzero. There are two ways to interpret the U(1) gauge field. Astrophysically, one expects the black hole gauge charge to be very small if the gauge field corresponds to the Standard Model (SM) electromagnetic field. On the contrary, one can consider this gauge field not as the usual electromagnetic field of the SM but instead an additional field that is simply a component of gravity. In that case, there exist no constraints in principle for the black hole charge, but it is natural to expect it should also be small. Regardless of these considerations, one can consider black holes in EMD theory as natural proxies to consider general fields describing gravity: the spin 0 scalar, the spin 1 gauge field, and the spin 2 metric field.

IV. RESULTS

In what follows, we discuss results obtained for single and binary black hole systems, which have been studied via numerical simulations. Our implementation of Eqs. (13)–(18), along with the BSSN equations coupled to the sources in Eqs. (19)–(21), adopts finite difference techniques satisfying summation by parts on a regular Cartesian grid [47,48]. All fields are discretized using a fourth order accurate scheme. The time evolution of the resulting equations is performed by using a third order accurate Runge-Kutta scheme [22,25]. We employ adaptive mesh refinement (AMR) via the HAD computational infrastructure. This provides distributed, Berger-Oliger style AMR [24,27] with full subcycling in time, with the inclusion of an improved treatment of artificial boundaries [49]. In addition, for cases with large values of α_0, and for which the field becomes fairly nonsmooth in the central area of each black hole, we adopt a more aggressive form of dissipation (essentially a high-pass filter) on the dilaton localized to those regions which lie well within the apparent horizon. This aggressive form of dissipation utilizes a second order form (in addition to the usual fourth order)

of Kreiss-Oliger dissipation, which effectively provides for a smaller transition frequency when considering the dissipation as a low-pass filter.

In our single black hole runs, we adopt a mass $M = 1$ and employ a Cartesian grid with extent $[-64, 64]^3$ with a base resolution of 81 equispaced points in each direction. There are six levels of concentric, fixed, finer meshes covering half the extent of each parent, such that the finest resolution is $h = 0.05$. For these runs, we employ the standard gauge driver with $\eta = 2/M$ where η is the standard gauge parameter of the Gamma driver coordinate choice.

In our binary black hole runs, we adopt $m_1 = m_2 = 1/2$ for the equal mass case or for the unequal case $m_1 = 0.5788$, $m_2 = 0.3852$. Our coarsest computational grid is defined over $[-204.8, 204.8]^3$, and each direction is covered with 81 uniformly spaced points. We additionally employ eight levels of refinement (with a 2:1 refinement ratio). The first two are fixed in $[-102.4, 102.4]^3$ and $[-34, 34]^3$, while the remaining six adapt dynamically through the shadow hierarchy, giving a finest resolution of $h = 0.02$. For these runs, we use the standard gauge driver but find that resolving the rapid dynamics of the merger requires choosing $\eta = 1/(m_1 + m_2)$.

A. Single black holes

We present first the behavior of the dilaton scalar field in spacetimes with a weakly charged single black hole. For a simple way to choose initial data and to explore the stability of the black hole, we choose for our initial data a black hole solution in GR to which we add a monopole electric (or magnetic) field (the asymptotic charge value of which is kept fixed). The dilaton is set to a constant equal to its asymptotic value, ϕ_0. This data do not correspond to a stationary solution, but they are consistent with the constraints to $\mathcal{O}(Q^2)$.

This initial data are evolved, and, after some transient behavior, the system generally settles into a stationary solution. This behavior can be appreciated in Fig. 2, which plots the central value of ϕ as a function of time for a number of different configurations. In particular, for small values of α_0, as the charge $q \equiv Q/M$ is increased, the magnitude of the dilaton increases quadratically (the figure rescales some of the curves to fit in the figure); similar behavior is observed when increasing the value of α_0, which induces a linear increase in the dilaton. This behavior is in agreement with the known solution described in Appendix A.

Also shown in the figure are the results of choosing a Gaussian profile for the dilaton at the initial time instead of a constant value. In particular, adopting a Gaussian centered at the origin results in essentially the same stationary solution, despite differences at early times. This agreement suggests that a unique, static hairy black hole, insensitive to the initial configuration of the dilaton, is an attractor.

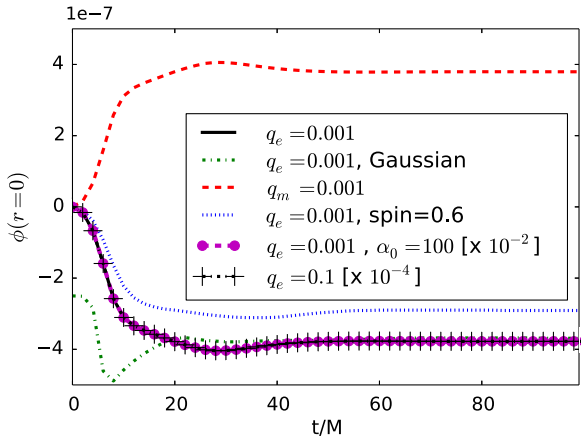

FIG. 2. Central value of dilaton scalar field as a function of time for various configurations of a single black hole. Note that the system generally settles to an apparently stationary configuration for some nontrivial profile of the dilaton field. Here, the asymptotic value of the scalar field for the electric cases is $\phi_0 = -10^{-10}$ and for the magnetic case is $\phi_0 = +10^{-10}$. For those not denoted otherwise, $\alpha_0 = 1$. The last two cases are rescaled as indicated to fit the scales of the plot. Note that the first case and the last two cases overlap one another.

Also included is one example of a spinning black hole with $a/M = 0.6$. Similar to the static case, our evolutions suggest a unique, stationary, rotating, stable hairy black hole. The effect of increasing α_0 and the spin are discussed below.

Finally, there is one case where a monopole magnetic field has been added to the black hole, showing that the dilaton is basically the same as in the electric case but with the opposite sign.

To analyze the solution in more detail, we focus on the case of a nonspinning, electrically charged black hole with $q_e \equiv Q_e/M = 10^{-3}$ and obtain the asymptotic dependence of the field which can be described by $\phi(r) \approx \phi_0 + \phi_1/r$. We stress that, in contrast to the behavior of the scalar field with neutron stars in scalar-tensor (ST) theories, the scalar charge ϕ_1 does not sensitively depend on the asymptotic value of the scalar field ϕ_0. This insensitivity implies that effects such as induced and dynamical scalarization are less significant in EMD than in ST theories [11,14].

In relation to the discussion in Appendix B, Fig. 3 shows the value of this scalar charge as a function of dilaton coupling α_0. Notice the linear behavior for small values of α_0, whereas a different trend is clear for larger values. This behavior can be extracted analytically from the solution presented in Appendix A (neglecting, for the moment, the asymptotic value of the dilaton), from which the scalar charge can be calculated as

$$\phi_1 = \frac{\alpha_0 Q_e^2}{M} \frac{1}{1 + \sqrt{1 + (\alpha_0^2 - 1) Q_e^2/M^2}}. \tag{38}$$

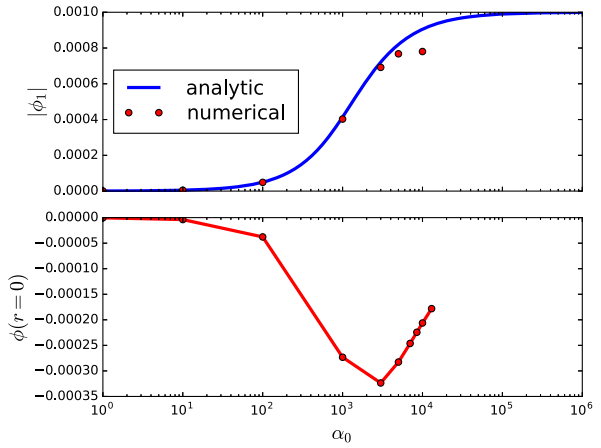

FIG. 3. Dilaton behavior for a single, electrically charged, nonspinning black hole with $q_e = 0.001$, $M = 1$, and $\phi_0 = -10^{-10}$. These quantities have been extracted at late times when the solution settled down to a roughly stationary solution. (Top) The dilaton scalar charge along with the analytic value, expression (38), for $q_e = 0.001$ and $M = 1$. (Bottom) The central value of the scalar field at late times.

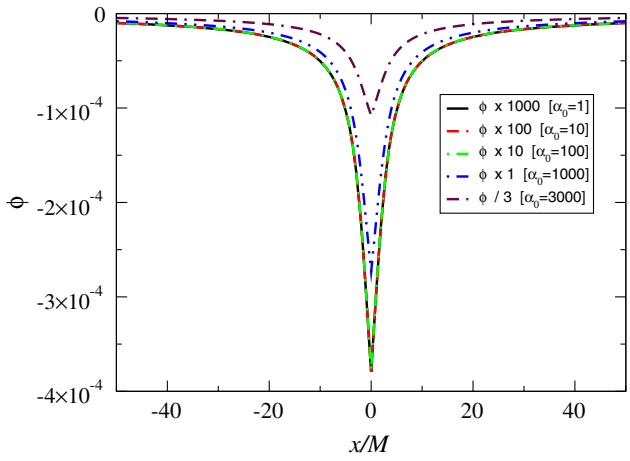

FIG. 4. The profile of the scalar field for different values of α_0 (with $q_e = 0.001, M = 1$, and $\phi_0 = 10^{-10}$). The profiles are rescaled assuming a linear increase with the coupling. For $\alpha_0 \lesssim 100$, this linear scaling is apparent.

The behavior at small α_0 extracted from Eq. (38) is $\phi_1 \approx \alpha_0 Q_e^2/(2M)$, while for large values, $\phi_1 \to |Q_e|$. The numerical solutions obtained for $\alpha_0 \lesssim 5000$ are in excellent agreement with this expression, while a lower than expected scalar charge is obtained above this value of α_0. We note, however, that numerical simulations become quite challenging at such large values. For this reason, we will restrict to $\alpha_0 \leq 3000$ when studying binary mergers [50].

We also monitor the central value of the scalar field and display its behavior for the electric case in the bottom panel of Fig. 3. Although the central field increases at small coupling, the trend changes dramatically around $\alpha_0 = 2000$, precisely the point at which the dilaton charge saturates. This behavior is yet another indication of a transition in the system as α_0 is increased.

Additional insights can be gained by examining the radial profile of the stationary solution and its dependence on the coupling α_0. Figure 4 shows the radial profile of the dilaton in the case that $\phi_0 = 10^{-10}, q_e = 10^{-3}$ and for $\alpha_0 = \{1, 10, 10^2, 10^3, 3 \times 10^3\}$. For comparison purposes, we rescale linearly the profiles with respect to the value $\alpha_0 = 1000$. That the solution scales linearly for small coupling is clearly apparent, in contrast to the solutions for large α_0.

Proceeding in a similar fashion for spinning black holes (keeping for concreteness $q_e = 0.001, \alpha_0 = 1$), we measure the scalar charge as we vary the spin parameter of the black hole in the range [0, 0.6] (to ensure a small initial constraint violation). We find that the scalar charge measured from the stationary state can be fit approximately as

$$\phi_1(a/M) = \phi_1(0)\left(1\text{–}0.4\left(\frac{a}{M}\right)^2\right), \tag{39}$$

where $\phi_1(a = 0)$ is the value of the scalar charge for the nonrotating case. Notice the charge *decreases* as the spin increases.

We have also looked at the quasinormal modes (QNM) of oscillation of perturbed black holes. In particular, on simulating the head-on collision of two black holes, we produce a strongly perturbed remnant black hole and can extract the frequency of the strongest QNM in the ringdown. Such QNM frequencies have been calculated analytically for $\alpha_0 = 1$ in EMD [31]. We confirm that the frequency from the numerical simulation agrees with the analytic value to within 4(7)% for the real (imaginary) part of the frequency.

However, we note that for the small (electromagnetic) charges that we consider here the differences in these QNM frequencies in comparison to the GR case are small not just for the $\alpha_0 = 1$ case but for a large range of α_0 values as well. In consequence, the difference in EMD and GR ringdown dynamics will not be distinguishable above our numerical error (of the order of 5% in the extracted frequency/decay rate of the fundamental mode). Another way of saying this is that the role of the dilaton is largely inconsequential in terms of its effect on the dynamics and the formation of the final black hole. This is consistent with our earlier observation that EMD, for different values of the coupling α_0, has a phenomenology that interpolates between charged and neutral black holes. Indeed, we could well have inferred the comparable QNM decay rates between EMD and GR from this observation and the known QNM spectra for weakly charged black holes [51–54].

B. Binary black holes

We now turn our attention to binary black hole systems both with equal and unequal masses. From our single black hole results, it is clear that observations made with small

values of the coupling α_0 have a simple scaling until $\alpha_0 \approx 10^3$ for the cases where the charge is $q_e = 10^{-3}$. We have studied the dynamics of binaries for a broad set of α_0 values and confirmed this expectation. In what follows, we thus concentrate on discussing the particular cases $\alpha_0 = \{1, 10^3, 3 \times 10^3\}$. Note that because of (i) the limitations of our initial data, (ii) a desire to take a conservative approach in this first study, and (iii) the expectation that astrophysical black holes are likely close to neutral—-even if the gauge field is not the one that couples to the Standard Model—we choose a small value of q_e.

For the nondimensionalized electric charge of $q_e = 10^{-3}$, the binaries orbit for four to five cycles before merging into a single spinning black hole. Figures 5 and 6 summarize our results for both equal and unequal mass (mass ratio $m_1/m_2 = 3/2$) cases. In each figure, the top panel shows the real part of the radiative Newman-Penrose scalar Ψ_4 for different values of α_0, and the middle panel displays the differences of their magnitudes with respect to the $\alpha_0 = 1$ case. The differences as indicated in the middle panels of Figs. 5 and 6 are small even for $\alpha_0 \gg 1$. They are clearly on the order of a few percent in amplitude (this has been confirmed through higher resolution runs, though we note the difference in phase is significantly larger up to values of $\simeq \pi$ across the resolutions employed in our tests).

The angular frequency of the dominant gravitational wave mode is shown in the bottom panel. Again, the differences with variations in α_0 are small. However, that the cases with larger coupling merge earlier (albeit very slightly) is consistent with the expectations that larger coupling will result in increased energy loss through scalar radiation.

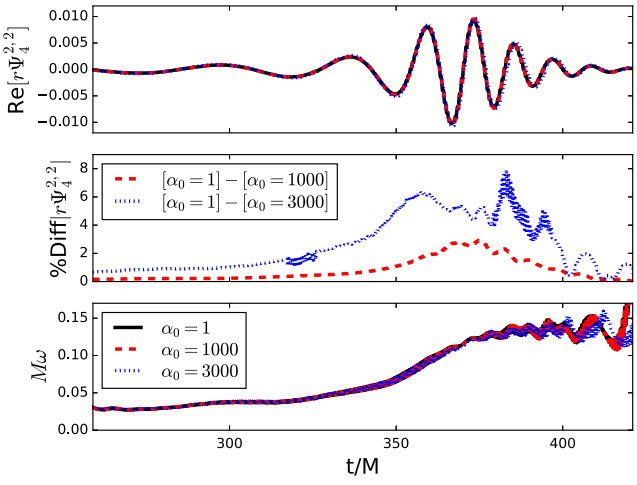

FIG. 5. The gravitational radiation of an equal mass binary black hole with an electric charge $q_e = 0.001$ for different values of α_0. Top: The real part of the $l = m = 2$ mode of the Newman-Penrose scalar Ψ_4. Middle: The percent difference in magnitude of the $l = m = 2$ mode of Ψ_4 relative to the α_1 case normalized by the maximum of the signal. Bottom: The angular frequency of the gravitational wave mode.

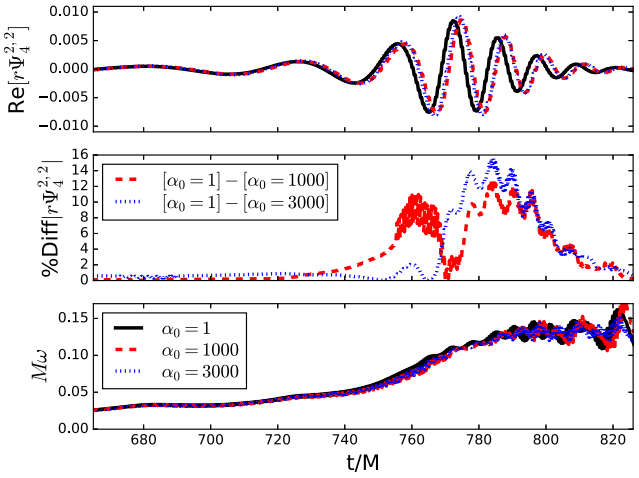

FIG. 6. The gravitational radiation of an unequal mass binary black hole with an electric charge $q_e = 0.001$ for different values of α_0. Top: The real part of the $l = m = 2$ mode of the Newman-Penrose scalar Ψ_4. Middle: The percent difference in magnitude of the $l = m = 2$ mode of Ψ_4 relative to the α_1 case normalized by the maximum of the signal. Bottom: The angular frequency of the gravitational wave mode.

Of course, even these small differences are possibly degenerate with other parameters. That is to say that the signals we find, were they to be measured by LIGO, would likely be mistaken for GR signals for a black hole binary with parameters somewhat different than those we adopt here. The binary mass in particular could probably be adjusted to generate GR waveforms that would be indistinguishable from these EMD waveforms. Recent examples proposing that LIGO's detections are perhaps more exotic than simply binary black hole mergers within GR include Refs. [55,56].

The observations that differences are small can also be inferred from multiple points of view; to wit:

(i) As noted in Appendix A, static black holes in EMD become neutral in the $\alpha_0 \to \infty$ limit. It is natural then to expect a similar limit for black holes in binaries, and this decreasing charge has implications for merger time. As demonstrated in Ref. [57], which studied the particular case of black hole binaries with the same sign of charge with $\alpha_0 = \sqrt{3}$ (following Ref. [58]), the estimated radius of the effective innermost stable circular orbit increases as the black hole charge increases. Following our observation that larger couplings have effectively smaller black hole charges, one expects that, for fixed charges of equal sign, black holes will merge sooner (i.e. at lower frequencies) for smaller coupling.

(ii) It is interesting to consider the behavior of binary neutron stars in scalar-tensor theories. In particular, the clearest differences in those simulations from those of GR occurred for scalar charges of the order $\phi_1 \approx 10^{-1}$. However, here the charges are a couple

orders of magnitude smaller, only $\phi_1 \approx 10^{-3}$, and one expects dynamical differences to scale with ϕ_1^2. And so perhaps it is natural that the differences we see for these parameter choices are as small as we report. Scalarization levels comparable to those neutron star mergers would require BH charges $\alpha_0 q^2 M \approx 10^{-1}$ ($qM \simeq 10^{-1}$) for small (very large) values of α_0.

Because EMD allows for scalar radiation, we can gain additional understanding by extracting it in addition to the gravitational wave signal. As discussed in Appendix B, the computation of the Newman-Penrose scalar Φ_{22} indicates that the scalar radiation is expected to scale as $\Phi_{22} \approx \alpha_0 \phi_{,tt}$ (evaluated asymptotically). One can thus estimate that this radiation in the early inspiral phase scales as $\Phi_{22} \approx \alpha_0 \phi_1 \Omega^2$. This scaling is assumed in Fig. 7, which shows Φ_{22} as a function of time for both the equal and unequal mass cases. In particular, because the orbital frequency differs only slightly with changes to α_0, the rescaling depends only on the coupling and scalar charge. The coupling value is straightforward, but the black hole scalar charge is chosen as the scalar charge of individual black holes in isolation. Thus, the scalar charges for equal mass binaries are chosen as $\phi_1 = \{-4.8 \times 10^{-7}, -4 \times 10^{-4}, -6.9 \times 10^{-4}\}$ while for unequal mass binaries, we choose masses and scalar charges to be (m_1, m_2): $\phi_1 = \{(-3,-2)\times 10^{-7}, (-2.4,-1.6)\times 10^{-4}, (-4.2,-2.7)\times 10^{-4}\}$ for $\alpha_0 = \{1, 10^3, 3 \times 10^3\}$ respectively [which are well approximated by the analytical expression Eq. (38)].

As shown in Fig. 7, reasonably good agreement with the expected scaling is obtained during the inspiral phase, but the scaling overestimates the magnitude of the radiation during the merger. The failure of the scaling during the merger indicates that the nonlinear behavior is less radiative

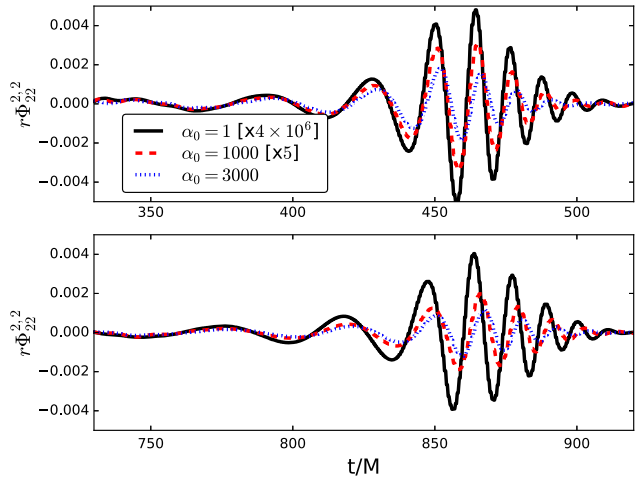

FIG. 7. The (real part of the) $l = m = 2$ mode of the scalar gravitational radiation Φ_{22} of a binary black hole with an electric charge $q_e = 0.001$ for different values of α_0. Top: The equal mass case. Bottom: The unequal mass case.

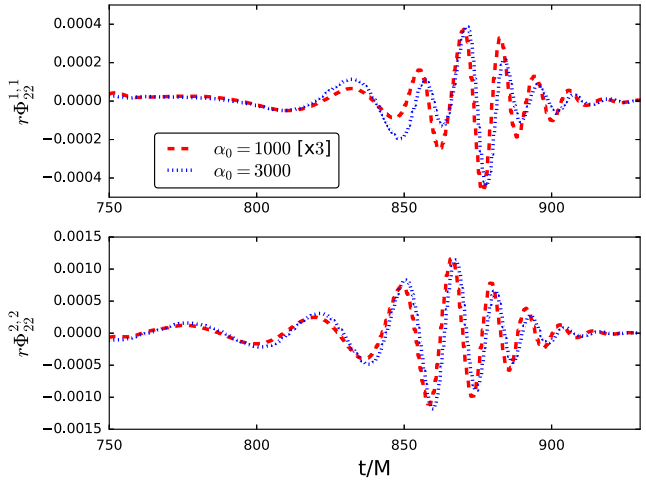

FIG. 8. The (real part of the) $l = m = 1$ and $l = m = 2$ modes of the scalar gravitational radiation Φ_{22} of a binary black hole with an electric charge $q_e = 0.001$ for different values of α_0 corresponding to the unequal mass binary case. Here, we have scaled up the case $\alpha_0 = 1000$ by a factor of 3 in accordance with expected scaling if the dilaton charge is ignored. Top: The $l = m = 1$ mode. Bottom: The $l = m = 2$ mode.

than otherwise expected from simple superposition arguments and is consistent with the observations made in the isolated black hole cases where the scalar charge shows a trend toward saturation at high coupling values.

This saturation is evident in Fig. 8, which shows the $l = m = 1$ and $l = m = 2$ modes for the scalar radiation corresponding to the unequal mass binary for $\alpha_0 = 1000$ and 3000. In contrast with Fig. 7, however, both cases here are scaled linearly by their respective value of α_0, ignoring the dilaton charge. Focusing only on the merger, this simple scaling in α_0 works quite well, supporting our assertion that the scalar charges saturate at large coupling.

An interesting aspect of gravitational radiation in EMD is that it could contain a dipolar component in contrast to GR, which disallows dipolar radiation. Although one generally expects the dipolar component, when allowed by the theory, to dominate over higher multipoles, here the strength of the dipolar component depends on the difference in the scalar charges of the black holes. As a result, the equal mass case produces no dipolar radiation. For the unequal mass binary with $m_1/m_2 = 3/2$ considered here, the scalar charges are different but nevertheless are sufficiently close to each other that the resulting $l = m = 1$ mode is weaker than the $l = m = 2$ mode.

We comment on two further conclusions that can be drawn from our studies as well as leave open a question deserving of investigation. First, we find the ringdown of the merger remnant appears largely insensitive to the value of the coupling. As mentioned in the previous section concerning the ringdown of the head-on remnant, small values of the electric charge produce correspondingly small differences in ringdown versus GR.

Second, we also studied the merger of black holes with electric charges of opposite sign. For the small electric charges considered here, no significant effect was observed on the black hole dynamics, indicating, as one might expect, that electromagnetic forces are subleading with respect to gravitational ones.

Finally, recall that the dilaton permits EMD black holes to have electric or magnetic charge (or both), and, as a result, these black holes have different properties. It could be interesting to consider the interaction of a binary black hole system comprised of one electrically charged and one magnetically charged black hole and investigate the impact on the dynamics and radiation. In particular, the black holes in such a binary would have scalar charges of opposite sign, which might maximize the resulting dipole scalar radiation. However, a preliminary investigation with the small charge used here did not reveal any dramatic effects.

V. FINAL DISCUSSION

We have examined the dynamics of black holes, both in isolation and in binaries, within Einstein-Maxwell-dilaton theory. We have focused on the differences between these dynamics and those in General Relativity.

This theory is parametrized by a coupling constant, α_0. For $\alpha_0 = 0$, the theory describes Einstein-Maxwell with a free scalar field, and its black hole solutions include Reissner-Nordstrom. The low energy limit of string theory is described by $\alpha_0 = 1$, which includes hairy black hole solutions. In the infinite coupling limit $\alpha_0 \to \infty$, the single, spherically symmetric, black hole solution is simply the Schwarzschild solution of pure vacuum General Relativity, and the electromagnetic field is essentially "screened" out.

Our results for binary mergers appear consistent with these same limits for isolated black holes. Of course, for $\alpha_0 = 0$, our black holes merge, producing a charged, hairless black hole. As α_0 is increased, the remnant black hole displays a scalar charge (in addition to its angular momentum and Maxwell charge).

The dynamics of both the dilaton and the gauge field are important and can impact the behavior of the dynamics of the binary. This influence is primarily governed by the strength of the scalar charge of the black hole which scales, at small coupling, as $\alpha_0 Q^2$. At large coupling, however, the scaling is such that the dilaton charge scales linearly with Q. For small values of Q, as we have seen, the effects are minor, while we expect large effects for larger values of Q.

Interestingly, because the scalar charge in EMD does not depend sensitively on the asymptotic value of the dilaton or the nearby charge of a companion (as opposed to the case in scalar-tensor theory [11,42]), its main role in equal mass binaries can be approximated by charged binary black hole mergers. Note that recent work argues that such black holes can undergo scalarization for sufficiently large values of the asymptotic value of the dilaton [59].

Considering again the case of large coupling, it is worth pointing out that the $\alpha_0 \to \infty$ limit is essentially a decoupling limit such that the gravitational dynamics and the matter (Maxwell and dilaton) dynamics have decreasing effects on one another. For large α_0, the matter fields are increasingly radiated away, while the scalar and electromagnetic contributions to the final black hole go to zero in this limit.

As discussed, for black holes in EMD, little has been known with regard to their stability properties, perturbation spectra for arbitrary coupling values, rotating solutions, etc. Our studies have shown that black holes in EMD have stability properties similar to those in GR. These results extend the analytical studies of Ref. [31] and highlight the small and subtle differences involved in distinguishing BHs in EMD and GR theories.

Finally, an immediate conclusion of our work is that for small charges differences with respect to waveforms in GR and EMD are quite small. Larger charges may well produce significant differences, and their main characteristics could be bracketed by analyzing charged/uncharged collisions in GR [60,61]. While one does not expect significantly charged black holes in the Universe, it is important to stress that the gauge field in EMD need not be the physical one coupled to the Standard Model.

ACKNOWLEDGMENTS

We thank Thibault Damour, William East, Matt Johnson, Paolo Pani, and Frans Pretorius as well as our longtime collaborators Mathew Anderson, David Neilsen, and Patrick Motl for interesting discussions. We also thank David Chow and Roman Konoplya for directing us to additional literature. This work has been supported in part by National Science Foundation (NSF) Grants No. PHY-1308727, No. PHY-1607356 (Brigham Young University), and No. PHY-1607291 (Long Island University), Natural Sciences and Engineering Research Council (NSERC), and CIFAR (L. L.) and the Spanish Ministry of Economy and Competitiveness Grant No. AYA2016-80289-P (AEI/FEDER,UE) to C. P. This research was enabled in part by support provided by scinet (www.scinethpc.ca) and Compute Canada (www.computecanada.ca). Research at Perimeter Institute is supported through Industry Canada and by the Province of Ontario through the Ministry of Research and Innovation.

APPENDIX A: EMD BLACK HOLE SOLUTIONS IN ISOTROPIC COORDINATES

Given our use of the BSSN formalism, isotropic coordinates are particularly useful. We present the spherically symmetric, static EMD black hole solutions here for reference. Defining a radial, isotropic coordinate, $\bar{r}$, via

$$r = \frac{1}{\bar{r}}\left[\left(\bar{r} + \frac{r_+ + r_-}{4}\right)^2 - \frac{r_+ r_-}{4}\right] \tag{A1}$$

for which

$$r_+ = M\left\{1+\left[1-(1-\alpha_0^2)\frac{Q^2}{M^2}\right]^{1/2}\right\} \tag{A2}$$

$$r_- = \frac{Q^2}{M}(1+\alpha_0^2)\left\{1+\left[1-(1-\alpha_0^2)\frac{Q^2}{M^2}\right]^{1/2}\right\}^{-1}, \tag{A3}$$

we can write the metric for both the magnetic and electric cases as

$$ds^2 = -\alpha^2 dt^2 + \chi^{-1}[d\bar{r}^2 + \bar{r}^2 d\Omega^2] \tag{A4}$$

$$= -\frac{(\bar{r}-\bar{r}_H)^2(\bar{r}+\bar{r}_H)^{2(1-\alpha_1)}}{(\bar{r}+\bar{r}_1)^{2-\alpha_1}(\bar{r}+\bar{r}_2)^{2-\alpha_1}}dt^2 + \frac{1}{\bar{r}^4}(\bar{r}+\bar{r}_1)^{2-\alpha_1}(\bar{r}+\bar{r}_2)^{2-\alpha_1}(\bar{r}+\bar{r}_H)^{2\alpha_1} \times [d\bar{r}^2 + \bar{r}^2 d\Omega^2]. \tag{A5}$$

Here, we have defined

$$\bar{r}_1 = \frac{1}{4}(\sqrt{r_+} - \sqrt{r_-})^2 \tag{A6}$$

$$\bar{r}_2 = \frac{1}{4}(\sqrt{r_+} + \sqrt{r_-})^2 \tag{A7}$$

$$\bar{r}_H = \frac{1}{4}(r_+ - r_-) \tag{A8}$$

with $\bar{r}_H$ the radial location of the horizon in these coordinates. If we consider the magnetic case, then $Q^2 = Q_m^2 e^{-2\alpha_0\phi_0}$, while for the electric case, $Q^2 = Q_e^2 e^{2\alpha_0\phi_0}$.

In the magnetic case, the EM and dilaton fields take the form

$$F_{\theta\phi} = Q_m \sin\theta \tag{A9}$$

$$B^{\bar{r}} = \frac{Q_m \bar{r}^4}{(\bar{r}+\bar{r}_H)^{3\alpha_1}}[(\bar{r}+\bar{r}_1)(\bar{r}+\bar{r}_2)]^{3(\alpha_1-2)/2} \tag{A10}$$

$$e^{-2\alpha_0\phi} = e^{-2\alpha_0\phi_0}\frac{(\bar{r}+\bar{r}_H)^{2\alpha_1}}{(\bar{r}+\bar{r}_1)^{\alpha_1}(\bar{r}+\bar{r}_2)^{\alpha_1}}. \tag{A11}$$

In the electric case, the EM and dilaton fields take the form

$$F_{t\bar{r}} = Q_e\frac{(\bar{r}^2-\bar{r}_H^2)}{(\bar{r}+\bar{r}_1)^2(\bar{r}+\bar{r}_2)^2} \tag{A12}$$

$$E^{\bar{r}} = -\frac{Q_e \bar{r}^4}{(\bar{r}+\bar{r}_H)^{\alpha_1}}[(\bar{r}+\bar{r}_1)(\bar{r}+\bar{r}_2)]^{(\alpha_1-6)/2} \tag{A13}$$

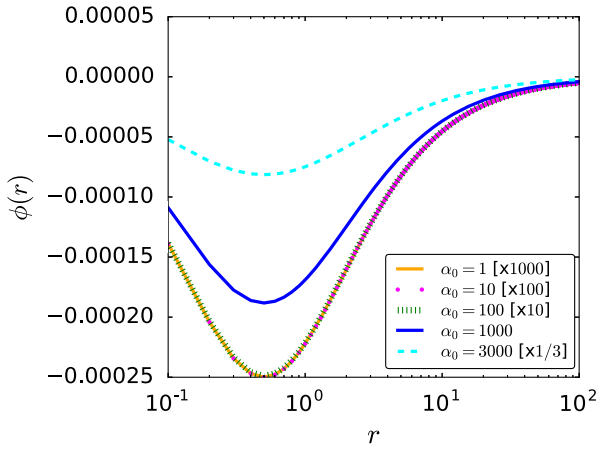

FIG. 9. Radial profile for the scalar field obtained in isotropic coordinates with different values of α_0 (all with $q_e = 10^{-3}, \phi_0 = 10^{-10}$). The solutions have been rescaled in the same way as the solutions in Fig. 4. This linear scaling holds only up to roughly $\alpha_0 \approx 100$.

$$e^{2\alpha_0\phi} = e^{2\alpha_0\phi_0}\frac{(\bar{r}+\bar{r}_H)^{2\alpha_1}}{(\bar{r}+\bar{r}_1)^{\alpha_1}(\bar{r}+\bar{r}_2)^{\alpha_1}}. \tag{A14}$$

For an illustration of the properties of the solution and a demonstration of the scaling with the coupling α_0, we plot the radial profile of ϕ versus the radius for different values of $\alpha_0 = \{1, 10^1, 10^2, 10^3, 3\times 10^3\}$ with fixed $q_e = 10^{-3}, \phi_0 = 10^{-10}$. To simplify the comparison, we scale all profiles linearly in α_0. As shown in Fig. 9, that the rescaled profiles for small α_0 coincide demonstrates that the solution does scale linearly in α_0, but the dependence of the solution on α_0 is milder at larger values.

The charge of these black holes is given by Eq. (38) and is plotted in Fig. 3 along with the charge obtained in our three-dimensional evolutions (in different coordinates). The figure makes clear that the charge saturates at large coupling.

APPENDIX B: CALCULATING RADIATIVE PROPERTIES OF THE SOLUTION

We recall that the physical frame is the Jordan one (the one with respect to which particles travel along geodesics). However, in our numerical studies, we find it convenient to compute the evolution in the Einstein frame. It is thus important to compute the radiative behavior in the Jordan frame, which, in particular, facilitates the comparison across the different cases considered.

Let us then analyze what a Jordan-frame observer would measure with respect to the Newman-Penrose radiative scalars obtained in the Einstein frame. First, recall our conformal transformation from the Jordan to the Einstein frame,

$$g^E_{ab} = g^J_{ab} e^{-2\alpha_0\phi} \equiv g^J_{ab}\Phi, \tag{B1}$$

where we introduce as a shorthand $\Phi \equiv e^{-2\alpha_0\phi}$. Next, given the standard null tetrad chosen in the Einstein frame T^E_α (with $\alpha = 0..3$ labeling the different null vectors of the tetrad), the Jordan frame tetrad is trivially related to the Einstein one by

$$T^E_\alpha = T^J_\alpha \sqrt{\Phi}. \tag{B2}$$

Now, to find the radiative (spin-2) scalar Ψ_4 in the Jordan frame computed from the Weyl tensor, we exploit the fact that the Weyl tensor, C^d_{abc}, is invariant with respect to conformal transformations; therefore, $C^E_{abcd} = C^J_{abcd}\Phi$ and, since Ψ_4 involves contractions with four tetrad members, we have—schematically—

$$\begin{aligned}\Psi^E &= C^E_{abcd} T^E T^E T^E T^E \\ &= C^J_{abcd} \Phi T^J T^J T^J T^J (\Phi)^{-2} \\ &= \Psi^J (\Phi)^{-1}.\end{aligned} \tag{B3}$$

Thus, $\Psi^J = \Psi^E e^{-2\alpha_0\phi}$.

We turn our attention now to the (spin-0) scalar radiation, which in the Newman-Penrose formalism is represented by the real scalar Φ_{22} and is obtained from the Riemann tensor. Recall that this tensor transforms under conformal transformations as

$$R^E_{ab} = R^J_{ab} - 2\nabla_a\nabla_b \ln\Phi + 2\nabla_a \ln\Phi \nabla_b \ln\Phi + g_{ab}\mathcal{S}, \tag{B4}$$

where $\mathcal{S}$ contains derivatives of Φ but will not contribute since $\Phi_{22} \equiv R_{ab}n^a n^b/2$ and n^a is a null vector (the same appearing in the calculation of Ψ_4). Proceeding as before, we obtain

$$\begin{aligned}\Phi^E_{22} &= R^E_{ab} T^E T^E/2 \\ &= R^E_{ab} T^J T^J/2(\Phi)^{-1} \\ &= (\Phi^J_{22} - n^a_J n^b_J \nabla_a \nabla_b \ln\Phi + \cdots)(\Phi)^{-1},\end{aligned} \tag{B5}$$

where we denote with … terms proportional to $(\ln\Phi)^2$ which will be subleading. Consequently, we have

$$\Phi^J_{22} = e^{-2\alpha_0\phi}(\Phi^E_{22} - 2\alpha_0 n^a_E n^b_E \nabla_a\nabla_b\phi). \tag{B6}$$

To estimate Φ^E_{22}, we can make use of the trace-reversed form of the Einstein equations in the Einstein frame (in what follows, we restrict to the Einstein frame, and we do not include a subindex) to obtain

$$\Phi^E_{22} = R_{ab}n^a n^b/2 = n^a n^b(\nabla_a\phi\nabla_b\phi + 2e^{-2\alpha_0\phi}F_{ac}F^c_b), \tag{B7}$$

where we have dropped terms involving $n^a n^b g_{ab}$. Furthermore, $n^a n^b F_{ac}F^c_b \propto r^{-2}$ as it can be written in terms of the Newman-Penrose scalar $\phi_2\bar{\phi}_2$. Therefore, the contribution of the Einstein-frame Φ_{22} is subleading with respect to the second term in the right-hand side of Eq. (B6). To leading order then, the scalar radiation, measured in the Jordan frame, scales as

$$\Phi^J_{22} \simeq \alpha_0 \phi_{,tt} e^{-2\alpha_0\phi}. \tag{B8}$$

As we have seen, for small values of the coupling α_0, the magnitude of the scalar charge ϕ_1 grows, but such growth saturates, and then it reverses at $\alpha_0 \simeq 3000$.

For a last step, one should be mindful of whether the asymptotic times measured in the different frames coincide. In all our simulations, we have chosen the asymptotic value of the scalar field to be (a small) constant ϕ_0. Upon transformation to the Jordan frame, this implies asymptotic observers carry clocks ticking at different rates given by $\kappa \equiv e^{\alpha_0\phi_0}$. Thus, we perform one last transformation to a single, common time, defined by $t \equiv \int \kappa dt'$, but for the couplings considered and the value of $\phi_0 = 10^{-10}$ adopted here, the correction is negligible.

[1] B. Abbott *et al.* (Virgo and LIGO Scientific Collaborations), Observation of Gravitational Waves from a Binary Black Hole Merger, Phys. Rev. Lett. **116**, 061102 (2016).

[2] B. Abbott *et al.* (Virgo and LIGO Scientific Collaborations), GW151226: Observation of Gravitational Waves from a 22-Solar-Mass Binary Black Hole Coalescence, Phys. Rev. Lett. **116**, 241103 (2016).

[3] B. P. Abbott *et al.* (Virgo Collaboration), GW170104: Observation of a 50-Solar-Mass Binary Black Hole Coalescence at Redshift 0.2, Phys. Rev. Lett. **118**, 221101 (2017).

[4] B. P. Abbott *et al.* (Virgo and LIGO Scientific Collaborations), Tests of General Relativity with GW150914, Phys. Rev. Lett. **116**, 221101 (2016).

[5] N. Yunes, K. Yagi, and F. Pretorius, Theoretical physics implications of the binary black-hole merger GW150914, Phys. Rev. D **94**, 084002 (2016).

[6] J. Meidam, M. Agathos, C. Van Den Broeck, J. Veitch, and B. S. Sathyaprakash, Testing the no-hair theorem with black hole ringdowns using TIGER, Phys. Rev. D **90**, 064009 (2014).

[7] E. Berti *et al.*, Testing general relativity with present and future astrophysical observations, Classical Quantum Gravity **32**, 243001 (2015).
[8] H. Yang, K. Yagi, J. Blackman, L. Lehner, V. Paschalidis, F. Pretorius, and N. Yunes, Black hole spectroscopy with coherent mode stacking, Phys. Rev. Lett. **118**, 161101 (2017).
[9] N. Yunes and F. Pretorius, Fundamental theoretical bias in gravitational wave astrophysics and the parameterized post-einsteinian framework, Phys. Rev. D **80**, 122003 (2009).
[10] M. Agathos, W. Del Pozzo, T. G. F. Li, C. Van Den Broeck, J. Veitch, and S. Vitale, TIGER: A data analysis pipeline for testing the strong-field dynamics of general relativity with gravitational wave signals from coalescing compact binaries, Phys. Rev. D **89**, 082001 (2014).
[11] E. Barausse, C. Palenzuela, M. Ponce, and L. Lehner, Neutron-star mergers in scalar-tensor theories of gravity, Phys. Rev. D **87**, 081506 (2013).
[12] M. Shibata, K. Taniguchi, H. Okawa, and A. Buonanno, Coalescence of binary neutron stars in a scalar-tensor theory of gravity, Phys. Rev. D **89**, 084005 (2014).
[13] E. Berti, V. Cardoso, L. Gualtieri, M. Horbatsch, and U. Sperhake, Numerical simulations of single and binary black holes in scalar-tensor theories: circumventing the no-hair theorem, Phys. Rev. D **87**, 124020 (2013).
[14] C. Palenzuela, E. Barausse, M. Ponce, and L. Lehner, Dynamical scalarization of neutron stars in scalar-tensor gravity theories, Phys. Rev. D **89**, 044024 (2014).
[15] B. P. Abbott *et al.* (Virgo and LIGO Scientific Collaborations), The rate of binary black hole mergers inferred from Advanced LIGO observations surrounding GW150914, Astrophys. J. **833**, L1 (2016).
[16] M. Okounkova, L. C. Stein, M. A. Scheel, and D. A. Hemberger, Numerical binary black hole mergers in dynamical Chern-Simons: I. Scalar field, Phys. Rev. D **96**, 044020 (2017).
[17] S. Endlich, V. Gorbenko, J. Huang, and L. Senatore, An effective formalism for testing extensions to General Relativity with gravitational waves, J. High Energy Phys. 09 (2017) 122.
[18] J. Cayuso, N. Ortiz, and L. Lehner, Fixing extensions to General Relativity in the non-linear regime, Phys. Rev. D **96**, 084043 (2017).
[19] D. Garfinkle, G. T. Horowitz, and A. Strominger, Charged black holes in string theory, Phys. Rev. D **43**, 3140 (1991); Erratum Phys. Rev. D **45**, 3888(E) (1992).
[20] V. P. Frolov, A. I. Zelnikov, and U. Bleyer, Charged rotating black hole from five-dimensional point of view, Ann. Phys. (Berlin) **499**, 371 (1987).
[21] J. H. Horne and G. T. Horowitz, Rotating dilaton black holes, Phys. Rev. D **46**, 1340 (1992).
[22] M. Anderson, E. Hirschmann, S. L. Liebling, and D. Neilsen, Relativistic MHD with adaptive mesh refinement, Classical Quantum Gravity **23**, 6503 (2006).
[23] C. Palenzuela, I. Olabarrieta, L. Lehner, and S. Liebling, Head-on collisions of boson stars, Phys. Rev. D **75**, 064005 (2007).
[24] S. L. Liebling, The singularity threshold of the nonlinear sigma model using 3d adaptive mesh refinement, Phys. Rev. D **66**, 041703 (2002).
[25] M. Anderson, E. W. Hirschmann, L. Lehner, S. L. Liebling, P. M. Motl, D. Neilsen, C. Palenzuela, and J. E. Tohline, Simulating binary neutron stars: dynamics and gravitational waves, Phys. Rev. D **77**, 024006 (2008).
[26] M. Anderson, E. W. Hirschmann, L. Lehner, S. L. Liebling, P. M. Motl, D. Neilsen, C. Palenzuela, and J. E. Tohline, Magnetized Neutron Star Mergers and Gravitational Wave Signals, Phys. Rev. Lett. **100**, 191101 (2008).
[27] HAD home page, http://had.liu.edu, 2010.
[28] M. Alcubierre, B. Bruegmann, P. Diener, M. Koppitz, D. Pollney, E. Seidel, and R. Takahashi, Gauge conditions for long term numerical black hole evolutions without excision, Phys. Rev. D **67**, 084023 (2003).
[29] G. W. Gibbons and K.-i. Maeda, Black holes and membranes in higher dimensional theories with dilaton fields, Nucl. Phys. **B298**, 741 (1988).
[30] G. T. Horowitz, in *Proceedings of string theory and quantum gravity '92, Triestre, Italy*, 1992, arXiv:hep-th/9210119.
[31] V. Ferrari, M. Pauri, and F. Piazza, Quasinormal modes of charged, dilaton black holes, Phys. Rev. D **63**, 064009 (2001).
[32] P. Bizon, Saddle point solutions in Yang-Mills dilaton theory, Phys. Rev. D **47**, 1656 (1993).
[33] D. Rasheed, The rotating dyonic black holes of Kaluza-Klein theory, Nucl. Phys. **B454**, 379 (1995).
[34] F. Larsen, Rotating Kaluza-Klein black holes, Nucl. Phys. **B575**, 211 (2000).
[35] B. Kleihaus, J. Kunz, and F. Navarro-Lerida, Global charges of stationary non-Abelian black holes, Phys. Rev. Lett. **90**, 171101 (2003).
[36] B. Kleihaus, J. Kunz, and F. Navarro-Lerida, Rotating dilaton black holes with hair, Phys. Rev. D **69**, 064028 (2004).
[37] B. Kleihaus, J. Kunz, and F. Navarro-Lerida, Stationary black holes with static and counter rotating horizons, Phys. Rev. D **69**, 081501 (2004).
[38] P. Aniceto, P. Pani, and J. V. Rocha, Radiating black holes in Einstein-Maxwell-dilaton theory and cosmic censorship violation, J. High Energy Phys. 05 (2016) 115.
[39] K. D. Kokkotas, R. A. Konoplya, and A. Zhidenko, Bifurcation of the quasinormal spectrum and zero damped modes for rotating dilatonic black holes, Phys. Rev. D **92**, 064022 (2015).
[40] R. Konoplya and A. Zhidenko, Detection of gravitational waves from black holes: Is there a window for alternative theories?, Phys. Lett. B **756**, 350 (2016).
[41] V. Cardoso, I. P. Carucci, P. Pani, and T. P. Sotiriou, Black holes with surrounding matter in scalar-tensor theories, Phys. Rev. Lett. **111**, 111101 (2013).
[42] T. Damour and G. Esposito-Farèse, Nonperturbative strong-field effects in tensor-scalar theories of gravitation, Phys. Rev. Lett. **70**, 2220 (1993).
[43] T. Damour and G. Esposito-Farese, Tensor-scalar gravity and binary pulsar experiments, Phys. Rev. D **54**, 1474 (1996).
[44] T. Damour and J. F. Donoghue, Equivalence principle violations and couplings of a light dilaton, Phys. Rev. D **82**, 084033 (2010).
[45] E. Poisson and C. M. Will, *Gravity* (Cambridge University Press, Cambridge, 2014).

[46] M. W. Horbatsch and C. P. Burgess, Cosmic black-hole hair growth and quasar OJ287, J. Cosmol. Astropart. Phys. 05 (2012) 010.
[47] G. Calabrese, L. Lehner, D. Neilsen, J. Pullin, O. Reula, O. Sarbach, and M. Tiglio, Novel finite-differencing techniques for numerical relativity: Application to black hole excision, Classical Quantum Gravity **20**, L245 (2003).
[48] G. Calabrese, L. Lehner, O. Reula, O. Sarbach, and M. Tiglio, Summation by parts and dissipation for domains with excised regions, Classical Quantum Gravity **21**, 5735 (2004).
[49] L. Lehner, S. L. Liebling, and O. Reula, AMR, stability and higher accuracy, Classical Quantum Gravity **23**, S421 (2006).
[50] Up to this value of the coupling, the analytic and late-time numerical solutions for the single BH agree.
[51] P. Pani, E. Berti, and L. Gualtieri, Gravitoelectromagnetic Perturbations of Kerr-Newman Black Holes: Stability and Isospectrality in the Slow-Rotation Limit, Phys. Rev. Lett. **110**, 241103 (2013).
[52] M. Zilhão, V. Cardoso, C. Herdeiro, L. Lehner, and U. Sperhake, Testing the nonlinear stability of kerr-newman black holes, Phys. Rev. D **90**, 124088 (2014).
[53] Z. Mark, H. Yang, A. Zimmerman, and Y. Chen, Quasinormal modes of weakly charged Kerr-Newman spacetimes, Phys. Rev. D **91**, 044025 (2015).
[54] O. J. C. Dias, M. Godazgar, and J. E. Santos, Linear Mode Stability of the Kerr-Newman Black Hole and Its Quasinormal Modes, Phys. Rev. Lett. **114**, 151101 (2015).
[55] J. W. Moffat, LIGO GW150914 and GW151226 gravitational wave detection and generalized gravitation theory (MOG), Phys. Lett. B **763**, 427 (2016).
[56] V. Cardoso, C. F. B. Macedo, P. Pani, and V. Ferrari, Black holes and gravitational waves in models of minicharged dark matter, J. Cosmol. Astropart. Phys. 05 (2016) 054.
[57] P. Jai-akson, A. Chatrabhuti, O. Evnin, and L. Lehner, Black hole merger estimates in Einstein-Maxwell and Einstein-Maxwell-dilaton gravity, Phys. Rev. D **96**, 044031 (2017).
[58] A. Buonanno, L. E. Kidder, and L. Lehner, Estimating the final spin of a binary black hole coalescence, Phys. Rev. D **77**, 026004 (2008).
[59] F.-L. Julié, On the motion of hairy black holes in Einstein-Maxwell-dilaton theories, J. Cosmol. Astropart. Phys. 01 (2018) 026.
[60] M. Zilhao, V. Cardoso, C. Herdeiro, L. Lehner, and U. Sperhake, Collisions of charged black holes, Phys. Rev. D **85**, 124062 (2012).
[61] S. L. Liebling and C. Palenzuela, Electromagnetic luminosity of the coalescence of charged black hole binaries, Phys. Rev. D **94**, 064046 (2016).